Organic Electronics 13 (2012) 43–52

Contents lists available at SciVerse ScienceDirect

Organic Electronics

journal homepage: www.elsevier.com/locate/orgel

Efficient non-doped blue light emitting diodes based on novel carbazole-substituted anthracene derivatives

Ying-Hsiao Chen [a], Shin-Lei Lin [b], Yu-Chen Chang [a], Yung-Chung Chen [c], Jiann-Tsuen Lin [c], Rong-Ho Lee [a,*], Wen-Jang Kuo [d], Ru-Jong Jeng [a,e,*]

[a] Department of Chemical Engineering, National Chung Hsing University, Taichung 402, Taiwan
[b] Material and Chemical Laboratories, Industrial Technology Research Institute, Hsinchu 310, Taiwan
[c] Institute of Chemistry, Academia Sinica, Taipei 115, Taiwan
[d] Department of Applied Chemistry, National University of Kaohsiung, Kaohsiung 811, Taiwan
[e] Institute of Polymer Science and Engineering, National Taiwan University, Taipei 106, Taiwan

ARTICLE INFO

Article history:
Received 10 June 2011
Received in revised form 25 August 2011
Accepted 3 October 2011
Available online 20 October 2011

Keywords:
Organic light-emitting diodes
Carbazole group
Anthracene derivative
Electroluminescence properties

ABSTRACT

In this study, we synthesized three anthracene derivatives featuring carbazole moieties as side groups – 2-*tert*-butyl-9,10-bis[4-(9-carbazolyl)phenyl]anthracene (Cz^9PhAnt), 2-*tert*-butyl-9,10-bis{4-[3,6-di-*tert*-butyl-(9-carbazolyl)]phenyl}anthracene (tCz^9PhAnt), and 2-*tert*-butyl-9,10-bis{4′-[3,6-di-*tert*-butyl-(9-carbazolyl)]biphenyl-4-yl}anthracene (tCz^9Ph_2Ant) – for use in blue organic light emitting devices (OLEDs). The anthracene derivatives presenting rigid and bulky *tert*-butyl-substituted carbazole units possessed high glass-transition temperatures (220 °C). Moreover, the three anthracene derivatives exhibited strong blue emissions in solution, with high quantum efficiencies (91%). We studied the electroluminescence (EL) properties of non-doped OLEDs incorporating these anthracene derivatives, with and without a hole-transporting layer (HTL). OLEDs incorporating an HTL provided superior EL performance than did those lacking the HTL. The highest brightness (6821 cd/m^2) was that for the tCz^9PhAnt-based device; the greatest current efficiency (2.1 cd/A) was that for the tCz^9Ph_2Ant-based device. The devices based on these carbazole-substituted anthracene derivatives also exhibited high color purity.

1. Introduction

Since Tang et al. first applied a light-emitting layer doped with a guest fluorescent dye to organic light-emitting devices (OLEDs), OLEDs have attracted growing interest for use in full-color flat-panel display applications and solid state lighting [1–6]. Although the photo-electronic properties of OLEDs have been investigated thoroughly and great advances have been made in developing novel organic light-emitting materials, high brightness and high current efficiency remain difficult to achieve for OLEDs based on blue emissive materials – due primarily to the carriers not being readily injected into the light-emitting layer of the device because of the large band gap energy of such materials. In addition to high brightness and high current efficiency, high color purity is also required for the full-color display applications [7–9]. Amorphous materials possessing high thermal stability are also needed to obtain OLEDs exhibiting excellent operational stability [10–12].

Several small-molecule emitters, including terfluorene [13], anthracene [14], distyrylarylene [15,16], carbazole, [17] and pyrene [18] derivatives, have been reported for applications in blue OLEDs. For example, a device based on 4,4′-bis(2,2-diphenylvinyl)-1,10-biphenyl (DPVBi) has exhibited a high luminous efficiency and a blue-greenish emission [15]. Unfortunately, the low glass transition temperature (T_g) of DPVBi led to the formation of crystals in the light-emitting layer, thereby resulting in poor operational

* Corresponding authors.
E-mail addresses: rhl@nchu.edu.tw (R.-H. Lee), rujong@ntu.edu.tw (R.-J. Jeng).

1566-1199/$ - see front matter © 2011 Elsevier B.V. All rights reserved.
doi:10.1016/j.orgel.2011.10.004

stability of the device [16]. A device based on another well-known blue-emitting material, 2-methyl-9,10-di (2-naphthyl)anthracene (MADN) [14], has exhibited superior thermal stability and higher color purity than those of the devices based on DPVBi, but its low luminance efficiency inhibits its potential application in full-color displays. Therefore, the development of novel organic light-emitting materials with high brightness, high current efficiency, high color purity, and good operational stability remains an important challenge for realizing full-color OLED applications. Among the several types of blue emitters that have been reported, anthracene derivatives have emerged as one of most relevant electroluminescent materials because of their high photoluminescence (PL) and electroluminescence (EL) quantum yields and good thermal stabilities [19–37]. Several anthracene derivatives presenting electron-donating or -withdrawing moieties at their 9 and 10 positions display hole-transporting/light-emitting [20,28,31,33,35–37] or electron-transporting/light-emitting [24,27] properties. A direct substitution of either strong electron-withdrawing or electron-donating groups at 9 and 10 positions changes the electron density on the anthracene ring and consequently enhances the conjugation length of the anthracene derivative [27]. Apart from that, the attachment of bulky side-groups to the anthracene core can prevent π–π^* stacking interactions of the molecules in the solid state and reduce self-quenching effects [35,36].

Various electron-donating and -accepting groups have been attached to *tert*-butyl substituted anthracene derivatives for use as blue emitters in OLEDs [19–21,34–37]. High morphological stability of thin films of anthracene derivatives has been observed after introduction of a *tert*-butyl unit at the C2 position of the anthracene moiety [36]. Moreover, attachment of electron-donating/hole-transporting groups on the electron-acceptor/electron-transporter anthracene core can enhance the PL performance of anthracene derivatives. Excellent EL performances have been observed for such OLEDs based on bipolar anthracene derivatives [35,36]. Nevertheless, the attachment of 4-(9-carbazolyl)phenyl carbazoles and 3,6-di-*tert*-butyl-substituted carbazole moieties on 2-*tert*-butyl-substituted anthracene cores have not been synthesized previously. We have reported carbazole-based fluorophores that exhibit both blue emissions and hole-transporting properties [38]. Incorporating a carbazole moiety into a molecular scaffold can significantly improve the glassy-state durability and thermal stability of an organic compound. Moreover, the 3, 6, and 9 positions of the carbazole moiety are readily functionalized, allowing fine-tuning of the electro-optical properties of the molecule [39–43]. *N*-Arylated carbazoles, in which a phenyl or naphthyl group is attached at the 9 position of the carbazole unit, have exhibited excellent thermal stability and EL properties in small-molecule OLEDs [44–46]. In this study, we synthesized three carbazole-substituted anthracene derivatives – 2-*tert*-butyl-9,10-bis[4-(9-carbazolyl)phenyl]anthracene (Cz^9PhAnt), 2-*tert*-butyl-9,10-bis{4-[3,6-di-*tert*-butyl-(9-carbazolyl)] phenyl} anthracene (tCz^9PhAnt), and 2-*tert*-butyl-9,10-bis{4′-[3,6-di-*tert*-butyl-(9-carbazolyl)]biphenyl-4-yl} anthracene (tCz^9Ph_2Ant) – for use as blue emitters in OLEDs. For tCz^9PhAnt and tCz^9Ph_2Ant, we expected attachment of the non-coplanar 3,6-di-*tert*-butyl-substituted carbazole moieties onto the 9 and 10 positions of the central anthracene core to inhibit molecular close packing in the solid state and thereby enhance the EL performance. We positioned the 3,6-di-*tert*-butyl-(9-carbazolyl)phenyl and 3,6-di-*tert*-butyl-(9-carbazolyl)biphenyl units on the 2-*tert*-butyl-substituted anthracene core to study the effect of the conjugation length of the side groups on the EL performance. Moreover, we also synthesized the 4-(9-carbazolyl)phenyl carbazole-substituted anthracene derivative Cz^9PhAnt for the sake of comparison. We expected to observe excellent EL performance from these carbazole-substituted anthracene derivatives. In addition, we analyzed the influence of the attached carbazole moieties on the thermal stability, electro-chemical properties, photophysical behavior, and EL performances of the anthracene derivative-based devices.

2. Experimental section

2.1. Materials

All reactions and manipulations were performed under a N_2 atmosphere using standard Schlenk techniques. All chromatographic separations were performed using SiO_2. 9*H*-Carbazole, copper powder, potassium carbonate, [18]crown-6 (18C6), 1,4-dibromobenzene, 4,4′-dibromobiphenyl, 2-chloro-2-methylpropane, nitromethane, zinc chloride ($ZnCl_2$), and *n*-butyl lithium (*n*-BuLi) were obtained from Aldrich and used as received. Potassium iodide and sodium hypophosphite monohydrate were purchased from Acros. Acetic acid and *o*-dichlorobenzene (DCB) were obtained from TEDIA. Tetrahydrofuran (THF) was purified through distillation from Na in the presence of benzophenone. The syntheses of compounds **1**–**4** and carbazole-substituted anthracene derivatives (Cz^9PhAnt, tCz^9PhAnt, tCz^9Ph_2Ant) are presented in Scheme 1.

2.2. Synthesis of monomers

2.2.1. 3,6-Di-tert-butyl-9H-carbazole (*1*)

2-Chloro-2-methylpropane (9.8 mL, 90 mmol) was added dropwise to a suspension of 9*H*-carbazole (4.9 g, 30 mmol) and $ZnCl_2$ (12.2 g, 90 mmol) in nitromethane (100 mL) and then the mixture was stirred for a further 6 h at room temperature, followed by partition between ethyl acetate and water. The organic layer was dried ($MgSO_4$) and the volatiles evaporated under reduced pressure. The residue was poured into MeOH and filtered off, to give a white solid (6.6 g, 81%). ^{1}H NMR (600 MHz, $CDCl_3$): δ (ppm) 8.20 (d, J = 2.1 Hz, 2H), 7.58 (br s, 1H), 7.56 (dd, J = 8.55, 1.80 Hz, 2H), 7.25 (d, J = 8.4 Hz, 2H), 1.57 (s, 18H). ^{13}C NMR (125 MHz, $CDCl_3$): δ (ppm) 142.14, 137.93, 123.46, 123.14, 116.07, 110.07, 34.66, 32.09. HRMS (m/z): calcd for $C_{20}H_{25}N$ 279.1987; found 279.1980. Anal. Calcd for $C_{20}H_{25}N$: C, 85.97; H, 9.02; N, 5.01. Found: C, 85.85; H, 9.01; N, 5.46.

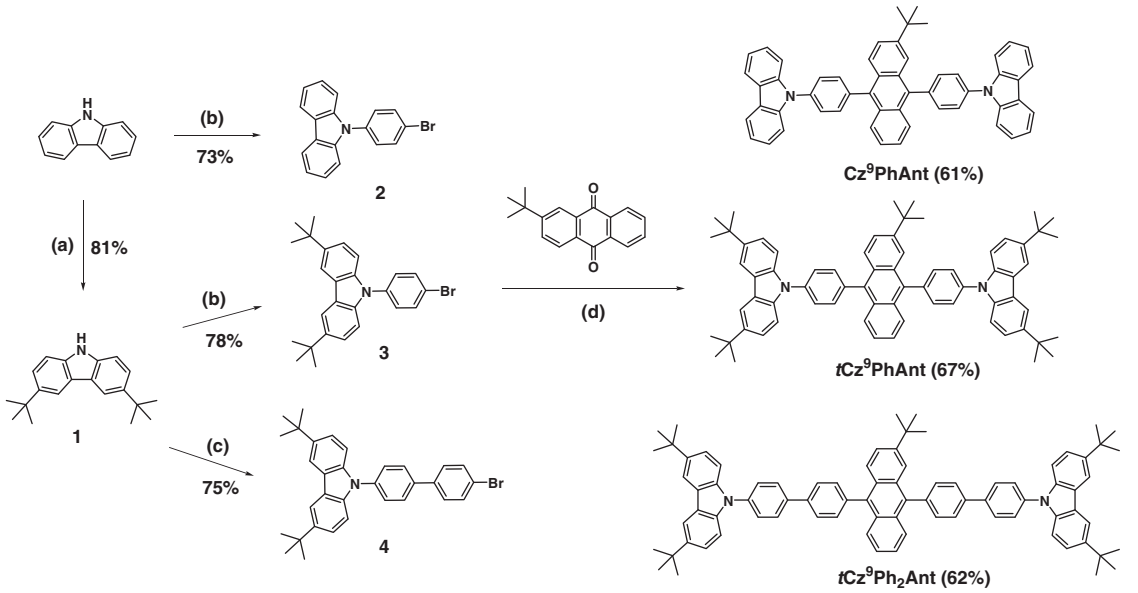

Scheme 1. Synthetic routes toward Cz^9PhAnt, tCz^9PhAnt, and tCz^9Ph_2Ant.

*2.2.2. 9-(4-Bromo-phenyl)-9H-carbazole (**2**)*

A mixture of 9*H*-carbazole (5.02 g, 30 mmol), 1,4-dibromobenzene (14.13 g, 60 mmol), K_2CO_3 (16.56 g, 120 mmol), Cu powder (1.94 g, 30 mmol), and 18C6 (3.71 g, 15 mmol) in *o*-DCB (120 mL) was stirred and deoxygenated under N_2 for 1 h and then the mixture was heated under reflux for a further 16 h. After cooling to room temperature, the crude mixture was filtered, and washed with CH_2Cl_2. The combined filtrates were evaporated to dryness and then the residues were subjected to column chromatography (SiO_2; hexane) to give a white solid (7.0 g, 73%). ^{1}H NMR (600 MHz, $CDCl_3$): δ (ppm) 8.13 (d, J = 7.8 Hz, 2H), 7.72 (d, J = 8.7 Hz, 2H), 7.40–7.45 (m, 3H), 7.35–7.38 (m, 3H), 7.26–7.31 (m, 2H). ^{13}C NMR (125 MHz, $CDCl_3$): δ (ppm) 140.60, 136.79, 133.10, 128.71, 126.07, 123.47, 120.87, 120.37, 120.20, 109.53. HRMS (*m*/*z*): calcd for $C_{18}H_{12}BrN$: 321.0153. Found: 321.0162. Anal. Calcd for $C_{18}H_{12}BrN$: C, 67.10; H, 3.75; N, 4.35. Found: C, 67.45; H, 3.73; N, 4.21.

*2.2.3. 3,6-Di-tert-butyl-9-(4-bromo-phenyl)-9H-carbazole (**3**)*

A mixture of **1** (5.6 g, 20 mmol), 1,4-dibromobenzene (15.7 g, 67 mmol), K_2CO_3 (11.1 g, 80 mmol), Cu powder (0.85 g, 13 mmol), and 18C6 (1.7 g, 6 mmol) in *o*-DCB (100 mL) was stirred and degassed under N_2 for 1 h and then heated under reflux for 12 h. After cooling to room temperature, the crude mixture was filtered, and washed with CH_2Cl_2. The combined filtrates were evaporated to dryness and then the residue was subjected to column chromatography (SiO_2; hexane/CH_2Cl_2, 7:3) to give a white solid (6.8 g, 78%). ^{1}H NMR (600 MHz, $CDCl_3$): δ (ppm) 8.18 (d, J = 1.50 Hz, 2H), 7.70 (dd, J = 8.70, 2.70 Hz, 2H), 7.49 (dd, J = 8.70, 1.80 Hz, 2H), 7.45 (dd, J = 8.70, 2.10 Hz, 2H), 7.33 (d, J = 8.4 Hz, 2H), 1.49 (s, 18H). ^{13}C NMR (125 MHz, $CDCl_3$): δ (ppm) 143.13, 138.90, 137.24, 132.93, 128.24, 123.71, 123.46, 120.22, 116.30, 108.96, 34.72, 31.98. HRMS (*m*/*z*): calcd for $C_{26}H_{28}BrN$ 433.1405; found 433.1409. Anal. Calcd for $C_{26}H_{28}BrN$: C, 71.89; H, 6.50; N, 3.22. Found: C, 71.94; H, 6.23; N, 3.55.

*2.2.4. 3,6-Di-tert-butyl-9-(4′-bromobiphenyl-4-yl)-9H-carbazole (**4**)*

A mixture of **1** (5.6 g, 20 mmol), 4,4′-dibromobiphenyl (12.5 g, 40 mmol), K_2CO_3 (11.1 g, 80 mmol), Cu powder (0.85 g, 13 mmol), and 18C6 (1.7 g, 6 mmol) in *o*-DCB (100 mL) was stirred and degassed under N_2 for 1 h and then heated under reflux with stirring for 12 h. After cooling to room temperature, the crude mixture was filtered and the collected solids washed with CH_2Cl_2. The combined filtrates were evaporated to dryness and the residue subjected to column chromatography (SiO_2; hexane/CH_2Cl_2, 3:1) to give a white solid (6.6 g, 64%). ^{1}H NMR (600 MHz, $CDCl_3$): δ (ppm) 8.18 (d, J = 1.2 Hz, 2H), 7.74 (d, J = 8.4 Hz, 2H), 7.63 (dd, J = 6.00, 3.60 Hz, 4H), 7.54 (d, J = 8.40 Hz, 2H), 7.50 (dd, J = 8.5, 2.10 Hz, 2H), 7.42 (d, J = 8.4 Hz, 2H), 1.49 (s, 18H). ^{13}C NMR (125 MHz, $CDCl_3$): δ (ppm) 142.98, 139.20, 139.07, 138.38, 137.72, 132.00, 128.62, 128.16, 126.95, 123.63, 123.45, 121.80, 116.27, 109.19, 34.73, 32.00. HRMS (*m*/*z*): calcd for $C_{32}H_{32}BrN$ 509.1718; found 509.1707. Anal. Calcd for $C_{32}H_{32}BrN$: C, 75.29; H, 6.32; N, 2.74. Found: C, 75.46; H, 6.28; N, 2.66.

2.2.5. 2-tert-Butyl-9,10-bis[4-(9-carbazolyl)phenyl]anthracene (Cz^9PhAnt)

A solution of **2** (3.22 g, 10 mmol) in dry THF (100 mL) was stirred at −78 °C and then *n*-BuLi (2.5 M in hexane, 4.8 mL) was added slowly over 1 h. A solution of 2-*tert*-

butylanthraquinone (1.32 g, 5.0 mmol) in THF (20 mL) was then added dropwise to the mixture at −78 °C. The resulting mixture was warmed to room temperature and stirred for overnight. After the reaction had finished, cold water was added to the mixture, which was then partitioned between EtOAc and water. The combined organic fractions were dried ($MgSO_4$) and the volatiles evaporated under reduced pressure. The residue was added to a mixture of KI (3.32 g, 20 mmol), sodium hypophosphite monohydrate (4.25 g, 40 mmol), and AcOH (50 mL) and then the mixture was heated under reflux for 5 h. After the reaction had finished, the mixture was poured into water and the precipitate filtered off and washed with plenty of water. The yellowish crude product was purified through column chromatography (SiO_2;hexane/CH_2Cl_2, 7:3) to give a white solid (2.2 g, 61%). ^{1}H NMR (600 MHz, $CDCl_3$): δ (ppm) 8.25 (d, J = 7.80 Hz, 4H), 7.91–7.99 (m, 3H), 7.84–7.88 (m, 4H), 7.78–7.81 (m, 4H), 7.63–7.76 (m, 6H), 7.49–7.58 (m, 6H), 7.39 (t, J = 7.8 Hz, 4H), 1.41 (s, 9H). ^{13}C NMR (125 MHz, $CDCl_3$): δ (ppm) 147.74, 140.97, 140.88, 138.47, 138.21, 137.07, 136.98, 136.16, 135.98, 132.84, 132.80, 130.09, 130.06, 129.69, 128.64, 127.04, 126.90, 126.84, 126.58, 126.06, 126.03, 125.31, 125.12, 123.55, 120.95, 120.43, 120.10, 120.08, 109.92, 109.80, 35.06, 30.72. HRMS (m/z): calcd for $C_{54}H_{40}N_2$ 716.3191; found 717.3287 $[M+1]^+$. Anal. Calcd for $C_{54}H_{40}N_2$: C, 90.47; H, 5.62; N, 3.91. Found: C, 90.60; H, 5.44; N, 3.22.

2.2.6. 2-tert-Butyl-9,10-bis{4-[3,6-di-tert-butyl-(9-carbazolyl)]phenyl}anthracene (tCz^{9}PhAnt)

tCz^{9}PhAnt was obtained as a white solid (3.1 g, 67%) after using a procedure similar to that described above for Cz^{9}PhAnt. ^{1}H NMR (600 MHz, $CDCl_3$): δ (ppm) 8.27 (s, 4H), 7.85–7.98 (m, 7H), 7.74–7.80 (m, 5H), 7.59–7.69 (m, 9H), 7.48–7.53 (m, 2H), 1.50 (s, 36H), 1.35 (s, 9H). ^{13}C NMR (125 MHz, $CDCl_3$): δ (ppm) 147.97, 143.33, 143.30, 139.64, 139.56, 138.24, 137.98, 137.89, 137.76, 136.55, 136.37, 133.03, 132.98, 130.41, 130.03, 128.97, 127.16, 126.93, 126.76, 125.55, 125.35, 124.03, 124.01, 123.87, 123.84, 121.33, 116.65, 109.71, 109.59, 35.37, 35.08, 32.37, 31.06. HRMS (m/z): calcd for $C_{70}H_{72}N_2$ 940.5696; found 941.5776 $[M+1]^+$. Anal. Calcd for $C_{70}H_{72}N_2$: C, 89.31; H, 7.71; N, 2.98. Found: C, 89.67; H, 7.53; N, 3.05.

2.2.7. 2-tert-Butyl-9,10-bis{4′-[3,6-di-tert-butyl-(9-carbazolyl)]biphenyl-4-yl}anthracene (tCz^{9}Ph$_2$Ant)

tCz^{9}Ph$_2$Ant was obtained as a white solid (3.4 g, 62%) after using a procedure similar to that described above for Cz^{9}PhAnt. ^{1}H NMR (600 MHz, $CDCl_3$): δ (ppm) 8.18 (s, 4H), 7.91–8.01 (m, 8H), 7.78–7.84 (m, 3H), 7.61–7.75 (m, 9H), 7.45–7.53 (m, 9H), 7.36–7.40 (m, 2H), 1.49 (s, 36H), 1.31 (s, 9H). ^{13}C NMR (125 MHz, $CDCl_3$): δ (ppm) 147.50, 142.95, 139.35, 139.31, 139.26, 139.11, 138.57, 138.48, 137.53, 136.52, 136.33, 132.01, 131.95, 130.16, 129.94, 129.69, 128.60, 128.36, 128.33, 127.06, 127.03, 127.00, 126.90, 126.74, 125.02, 124.83, 124.76, 123.67, 123.49, 121.19, 116.28, 109.32, 35.01, 34.76, 32.05, 30.83. HRMS (m/z): calcd for $C_{82}H_{80}N_2$ 1092.6322; found 1093.9395 $[M+1]^+$. Anal. Calcd for $C_{82}H_{80}N_2$: C, 90.06; H, 7.37; N, 2.56. Found: C, 90.17; H, 6.98; N, 2.55.

2.3. Measurements

^{1}H and ^{13}C NMR spectra were recorded using a Varian Gemini NMR spectrometer operated at 600 and 125 MHz, respectively. Elemental analysis was performed using an elemental analyzer (Elementar Vario EL III). High-resolution mass spectra were recorded using a Finnigan/Thermo Quest MAT mass spectrometer. Glass transition temperatures were measured under N_2 using a differential scanning calorimeter (TechMax Instruments DSC 6220) operated at a heating rate of 10 °C min^{-1}. Thermogravimetric analysis (TGA) was performed under a N_2 atmosphere using a thermogravimetric analyzer (VersaTherm thermogravimetric analyzer) operated at a heating rate of 10 °C min^{-1}. UV–vis absorption and PL spectra were recorded using a Shimadzu UV-1240 spectrophotometer and an Acton Research Spectra Pro-150 spectrometer, respectively. Cyclic voltammetry (CV) was conducted using a CHI model611D apparatus and a three-electrode cell, in which an indium tin oxide (ITO) sheet, a Pt wire, and silver/silver nitrate (Ag/Ag^+) were used as the working electrode, counter electrode, and reference electrode, respectively. All electrochemical experiments were performed using deoxygenated MeCN solutions containing 0.1 M tetrabutylammonium perchlorate (TBAP) as the electrolyte.

2.4. EL device fabrication and electro-optical characterization

Fabrication of OLEDs was conducted through high-vacuum thermal evaporation of the organic materials onto ITO-coated glass (sheet resistance: 15 Ω/square; Applied Film Corp.). Glass substrates with patterned ITO electrodes were washed well and then cleaned through O_2 plasma treatment. Furthermore, a LiF layer was thermally deposited onto the organic material layer, followed by Al metal deposition as the top layer in a high-vacuum chamber. The OLED configurations in this study were (type-A) ITO/anthracene derivative (70 nm)/1,3,5-tris(N-phenyl benzimidizol-2-yl)benzene (TPBI, 30 nm)/LiF (0.5 nm)/Al (150 nm) and (type-B) ITO/4,4′-bis[N-(1-naphthyl)-N-phenylamino]biphenyl (NPB, 40 nm)/anthracene derivative (30 nm)/TPBI (30 nm)/LiF (0.5 nm)/Al (150 nm), where NPB, the anthracene derivative, and TPBI were the hole-transporting layer (HTL), blue emitting layer, and electron-transporting layer (ETL), respectively. The cathode deposition rate was determined using a quartz thickness monitor (STM-100/MF, Sycon). The thin film thickness was determined using a surface texture analysis system (3030ST, Dektak). UV–vis spectra of the organic thin films were measured using a Hewlett–Packard 8453 spectrometer equipped with a photodiode array detector. PL and EL spectra were recorded using a Hitachi F-4500 fluorescence spectrophotometer. Current–voltage characteristics were measured using a programmable electrometer equipped with current and voltage sources (Keithley 2400). Luminance was measured using a Newport 1835C optical

meter equipped with a Newport 818-ST silicon photodiode.

3. Results and discussion

3.1. Synthesis and characterization

Scheme 1 illustrates the routes that we followed for the syntheses of the anthracene derivatives containing carbazole moieties. We obtained 3,6-di(*tert*-butyl)-9*H*-carbazole (**1**) through Friedel–Crafts alkylation of 9*H*-carbazole [47] and compounds **2**–**4** through Ullman coupling reactions [39]. The carbazole-containing anthracene derivatives Cz^9PhAnt, tCz^9PhAnt, and tCz^9Ph_2Ant were synthesized through reactions of 2-*tert*-butylanthraquinone with various carbazole derivatives [20]. ^1H and ^{13}C NMR spectroscopy, elemental analysis, and high-resolution mass spectrometry confirmed the chemical structures of these compounds. The relative intensities of the signals in the various spectra were in agreement with the proposed structures of these anthracene derivatives.

The operational stability of an OLED is directly related to the thermal stability of its light-emitting layer. Thus, high glass transition (T_g) and thermal degradation (T_d) temperatures are desirable for a light-emitting material to be applied in OLEDs. Fig. 1 presents DSC and TGA thermograms of the carbazole-substituted anthracene derivatives; Table 1 summarizes their values of T_g, crystallization temperature (T_c), melting temperature (T_m), and T_d The glass transition, and re-crystallization and melting peaks were clearly observed in the heating-scan, while only glass transition was observed during the cooling-scan for three anthracene derivatives. tCz^9Ph_2Ant exhibited values of T_d and T_g of 505 and 220 °C, respectively; among our three materials, these values were the highest, presumably because of the higher molecular weight of tCz^9Ph_2Ant [20]. The values of T_g, T_c, T_m, and T_d of Cz^9PhAnt were 168, 244, 355, and 490 °C, respectively. In contrast, tCz^9PhAnt exhibited only values of T_g and T_d (153 and 353 °C, respectively), but no signs of crystallization or melting. Presumably, the tight molecular stacking of Cz^9PhAnt in the absence of the *tert*-butyl groups on the 3 and 6 positions of carbazole unit meant that it exhibited thermal properties superior to those of tCz^9PhAnt. Furthermore, the presence of the sterically bulky carbazole side groups meant that these carbazole-substituted anthracene derivatives exhibited higher values of T_g than those of the well-known blue-emitting materials DPVBi (64 °C) [12] and MADN (120 °C) [14]. Therefore, we expected these carbazole-substituted anthracene derivatives to form the morphologically stable and uniform amorphous films required to improve the efficiencies and lifetimes of OLEDs.

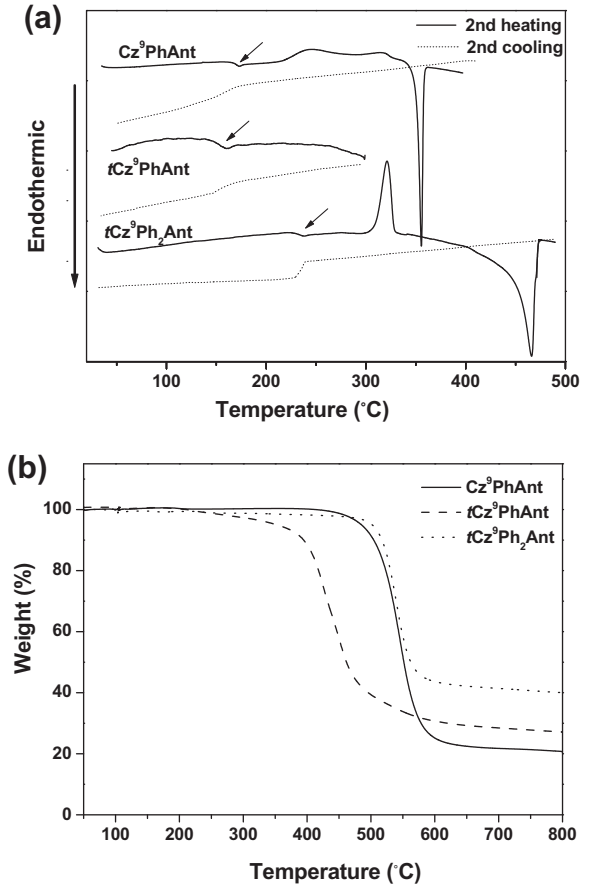

Fig. 1. DSC and TGA thermograms of Cz^9PhAnt, tCz^9PhAnt, and tCz^9Ph_2Ant.

3.2. Photophysical properties

Fig. 2 presents UV–vis absorption and PL spectra of the carbazole-substituted anthracene derivatives in dilute toluene solutions and as solid films. The UV–vis absorption spectra of the emitters in solution were measured at a concentration of 1 mg mL^{-1}; the thickness of the emitter layer for the UV–vis absorption measurements was approximately 100 nm. Table 1 summarizes the maximal absorption and PL emission wavelengths of the anthracene derivatives. The maximal absorption wavelengths of the anthracene derivatives appeared in the range from 280 to 320 nm (due to carbazole-centered transitions [48]), with moderately weak absorptions in the ranged from 350 to 425 nm (characteristic vibronic patterns attributed to the π–π^* transition of anthracene [26]). Relative to the absorption behavior of the anthracene derivatives in solution, the maximal absorption wavelengths corresponding to the carbazole-centered transitions were slightly red-shifted for the three anthracene derivatives in thin film state, presumably because of the interactions and aggregation of the molecules in thin film state.

Upon excitation at 350 nm, these anthracene derivatives exhibited deep-blue emissions with PL maxima at *ca.* 433–436 nm in dilute toluene solution. The maximum emission wavelength of the PL (λ_{max}^{PL}) and the full width at half-maximum (FWHM) of the PL were dependent on the chemical structure of the carbazole-substituted anthracene derivative. Relative to the PL spectra of the dilute solutions, however, the emission spectra of these anthracene derivatives exhibited red-shifts of 10–12 nm in the thin film state.

Table 1
Thermal and optical properties of the anthracene derivatives.

Compound	$T_g/T_c/T_m/T_d$ (°C)[a]	λ_{max}^{abs} (nm)[c]	λ_{max}^{PL} (nm)[c]	FWHM of λ_{max}^{PL} (nm)[c]	λ_{max}^{abs} (nm)[d]	λ_{max}^{PL} (nm)[d]	FWHM of λ_{max}^{PL} (nm)[d]	Φ_{fl} (%)[e]
Cz^9PhAnt	168/244/355/490	293	433	53	299	443	62	78
tCz^9PhAnt	153/n.a.[b]/n.a./353	298	433	55	299	444	55	70
$tCz9Ph_2$Ant	220/322/468/506	295	436	54	300	448	63	91

[a] All of the transition temperatures were determined form the second heating scan.
[b] n.a.: Not available.
[c] Measured in dilute toluene solution.
[d] Measured in solid film.
[e] PL quantum efficiency (Φ_{fl}) of the compounds, measured in toluene solution using 9,10-diphenylanthracene as a standard.

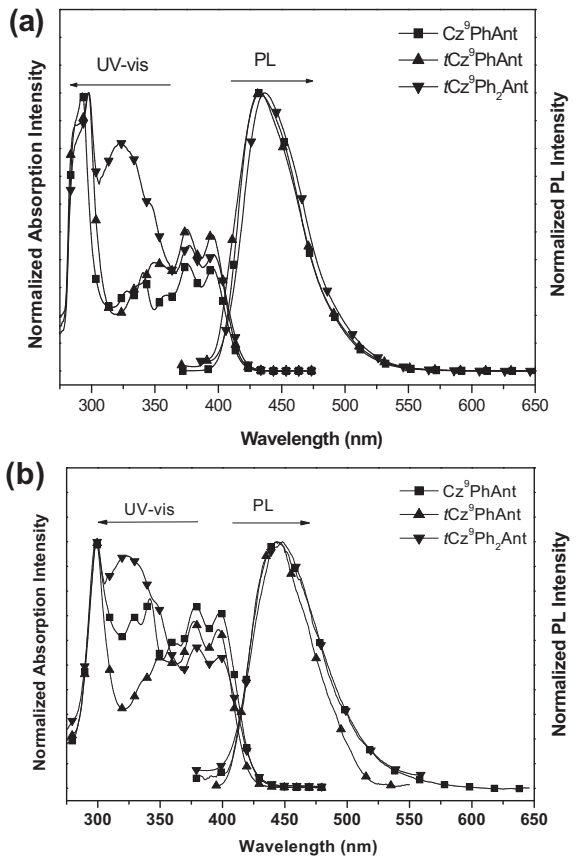

Fig. 2. UV–vis absorption and PL spectra of Cz^9PhAnt, tCz^9PhAnt, and tCz^9Ph_2Ant (a) in toluene solutions and (b) as thin films.

The differences in the PL spectra of the compounds in solution and in the form of thin films suggested the presence of intermolecular interactions or aggregation in thin film states. In the thin film, with the incorporation the *tert*-butyl substituents at the 3 and 6 positions of the carbazole unit, the value of λ_{max}^{PL} of tCz^9PhAnt was similar to that of Cz^9PhAnt, but the FWHM of tCz^9PhAnt was smaller than that of Cz^9PhAnt. The PL emission intensity of tCz^9PhAnt in the long wavelength range (450–550 nm) was weaker than that of Cz^9PhAnt. The steric hindrance of the *tert*-butyl groups on the peripheral carbazole group reduced the degree of intermolecular π–π stacking of tCz^9PhAnt, leading to the lower FWHM of the PL emission band. In addition, the value of λ_{max}^{PL} of tCz^9Ph_2Ant was slightly red-shifted (by 4 nm) relative to that of tCz^9PhAnt. The FWHM of the PL emission band was larger for tCz^9Ph_2Ant than it was for tCz^9PhAnt, presumably because tCz^9Ph_2Ant has one more benzene ring in its carbazole-substituted group than does tCz^9PhAnt; that is, the longer conjugation length led to the red-shift of the PL emission band of tCz^9Ph_2Ant. Moreover, the presence of the biphenyl groups made tCz^9Ph_2Ant more bulky, which would reduce conformation uniformity. As a result, the FWHM of tCz^9Ph_2Ant was larger than that of tCz^9PhAnt.

We measured the fluorescence quantum yields (Φ_{fl}) of the three anthracene derivatives in dilute toluene solution by comparing their emissions with that of a standard solution of 9,10-diphenylanthracene in cyclohexane (Φ_{fl} = 0.90) at room temperature [37]. Our blue emitters Cz^9PhAnt, tCz^9PhAnt, and tCz^9Ph_2Ant exhibited high quantum yields of 0.78, 0.70, and 0.91, respectively. We suspect that the value of Φ_{fl} of tCz^9PhAnt was smaller than that of Cz^9PhAnt because the vibration of the *tert*-butyl groups on the peripheral carbazole moiety resulted in the PL emission quenching of carbazole-substituted anthracene derivative. Nevertheless, the effect of the *tert*-butyl group was minimized after incorporation of the biphenyl group in the carbazole moiety. The greater conjugation length of the biphenyl-containing carbazole moiety led to the higher value of Φ_{fl} for tCz^9PhAnt relative to those of Cz^9PhAnt and tCz^9PhAnt. In addition, the presence of bipolar structure in these carbazole-attached 2-*tert*-butyl-substituted anthracenes would lead to larger Φ_{fl} values when compared with 2-*tert*-butyl-substituted anthracene derivatives [20,21,36].

3.3. Electrochemical properties of carbazole-substituted anthracene derivatives

We employed CV to investigate the electrochemical behavior of our compounds and to estimate the energy levels of the highest occupied molecular orbital (HOMO) and lowest unoccupied molecular orbital (LUMO) of the anthracene derivatives. The HOMO energy levels of the anthracene derivatives were calculated from the onset potential of oxidation (E_{onset}^{ox}) by assuming the absolute energy level of ferrocene was −4.8 eV below the vacuum level. Moreover, we calculated the LUMO energy levels from the HOMO energy levels and the absorption edges [48–50]. Fig. 3 presents the CV traces of 9,10-diphenylanthracene (DPA), Cz^9PhAnt, tCz^9PhAnt, and tCz^9Ph_2Ant, whereas Table 2 lists the band gap energies and LUMO

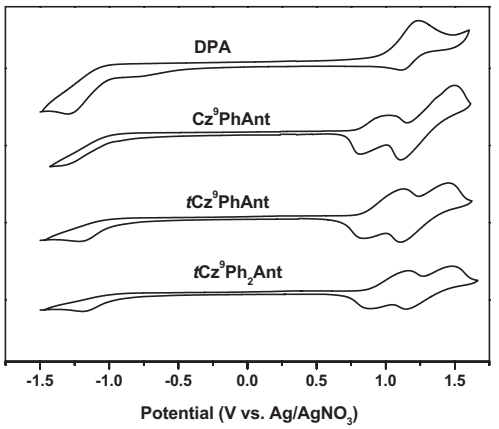

Fig. 3. CV spectra of DPA, Cz^9PhAnt, tCz^{9}PhAnt, and tCz^{9}Ph$_2$Ant.

Table 2
Electrochemical properties of the anthracene derivatives.

Compound	E_{ox} (V)[a]	HOMO (eV)	LUMO (eV)	E_g^{opt} (eV)[b]
Cz^9PhAnt	0.80	−5.47	−2.52	2.95
tCz^{9}PhAnt	0.85	−5.48	−2.53	2.95
tCz^{9}Ph$_2$Ant	0.86	−5.48	−2.57	2.91

[a] Onset oxidation potential versus Ag/AgNO$_3$.
[b] Calculated from the UV–vis absorption edge in dilute toluene solution.

and HOMO energy levels. For DPA, we found an oxidation peak and a reduction peak at about 1.25 and −1.25 V, respectively. The redox peaks were attributed to the oxidation/reduction of phenyl-substituted anthracene for DPA. Workentin et al. reported that a radical cation formed during the oxidation of DPA [51]. In addition, the carbazole-substituted anthracene derivatives exhibited two quasi-reversible oxidation peaks in the positive potential region. We attribute the oxidation peak at a lower potential to the oxidation of anthracene-linked carbazole unit. This is because the carbazole moiety is an electron-rich group [52]. Moreover, the oxidation peak of DPA showed up at a higher potential than the first oxidation peak of carbazole-substituted anthracene derivatives. Yet, the oxidation potential of the second oxidation peak was slightly higher than that of the oxidation peak of DPA. Therefore, we assigned the second oxidation peak, occurring at a more positive potential, to oxidation of the other carbazole unit in the anthracene derivative. This is because the second oxidation potential of carbazole-substituted anthracene would be enhanced as the first oxidation of carbazole moiety had been occurred. Two oxidation peaks were not assigned to the oxidation of two carbazole units and anthracene, respectively. This is because the current density ratio of two oxidation peaks was not 2:1. On the other hand, only one reduction peak was observed at about −1.25 V for the carbazole-substituted anthracene derivatives. The presence of the reduction peak in CV indicates that such anthracene derivatives exhibited the electron-accepting capacity, and could transport electrons when used as the emitter layer. The HOMO energy levels of Cz^9PhAnt, tCz^{9}PhAnt, and tCz^{9}Ph$_2$Ant were −5.47, −5.48, and −5.48 eV, respectively. The HOMO energy levels of carbazole-substituted anthracene derivatives are slightly higher than those of 9,10-di(2-naphthyl)anthracene (ADN, −5.8 eV) and 2-methyl-9,10-di(2′-naphthyl)anthracene (MADN, −5.5 eV) [24,33]. The incorporation of electron-rich carbazole moieties onto the 9 and 10 positions of anthracene enhances the HOMO energy levels of anthracene derivatives [38]. The high HOMO energy levels of carbazole-substituted anthracene derivatives facilitate hole-injection from an ITO transparent anode to the light-emitting layer [53]. As a result, we expected good EL performances from OLEDs based on our carbazole-substituted anthracene derivatives. The LUMO energy levels of Cz^9PhAnt, tCz^{9}PhAnt, and tCz^{9}Ph$_2$Ant were −2.52, −2.53, and −2.57 eV, respectively. The difference between the LUMO energy levels of the anthracene derivatives and TPBI (2.70 eV) was smaller than that between the anthracene derivatives and Alq_3 (3.30 eV) [20]. TPBI exhibits superior electron-injection characteristics than those of Alq_3. Moreover, the difference between the HOMO energy levels of the anthracene derivatives (5.48 eV) and TPBI (6.20 eV) is larger than that between the anthracene derivatives and Alq_3 (5.70 eV). TPBI shows a better hole-blocking characteristic than Alq_3 [54]. Consequently, superior EL performance could be realized if TPBI were to be used as the ETL in OLEDs based on these anthracene derivatives. The band gap energies of Cz^9PhAnt, tCz^{9}PhAnt, and tCz^{9}Ph$_2$Ant were 2.95, 2.95, and 2.91 eV, respectively. We suspect that the anthracene derivative tCz^{9}Ph$_2$Ant had a lower band gap energy than Cz^9PhAnt or tCz^{9}PhAnt because its carbazole moiety-based side groups featured a greater conjugation length [35]. Moreover, we expected good color purities for the blue emissions from OLEDs fabricated from anthracene derivatives with such large band gap energies.

3.4. EL properties of devices based on carbazole-substituted anthracene derivatives

According to their photophysical and electrochemical properties, the fluorophores Cz^9PhAnt, tCz^{9}PhAnt, and tCz^{9}Ph$_2$Ant appeared to be promising blue-emitting materials for OLED applications. To determine the EL properties of these fluorophores, we fabricated non-doped devices possessing double- and triple-layer configurations. In the double-layer devices (type-A devices; devices A-I, A-II, and A-III), the anthracene derivatives functioned as both the HTL and the blue emitting layer and TPBI functioned as both the hole-blocking material and the ETL. In the triple-layer devices (type-B devices; devices B-I, B-II, and B-III), NPB and the anthracene derivatives functioned as the HTL and blue emitting layer, respectively, while TPBI functioned as both the hole-blocking material and the ETL. Fig. 4 presents the configurations and energy levels of the double- and triple-layer devices, revealing that the OLEDs based on the anthracene derivatives possessed good matching of the energy levels at the interfaces between the HTL and the blue emitting layer and between the blue emitting layer and the TPBI layer.

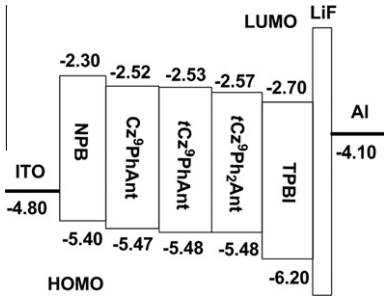

Fig. 4. Energy levels of the multilayer devices incorporating the fluorophores Cz^9PhAnt, tCz^9PhAnt, and tCz^9Ph_2Ant as emitting layers, NPB as the hole transporting layer, TPBI as the electron-transporting layer, and LiF as the buffer layer.

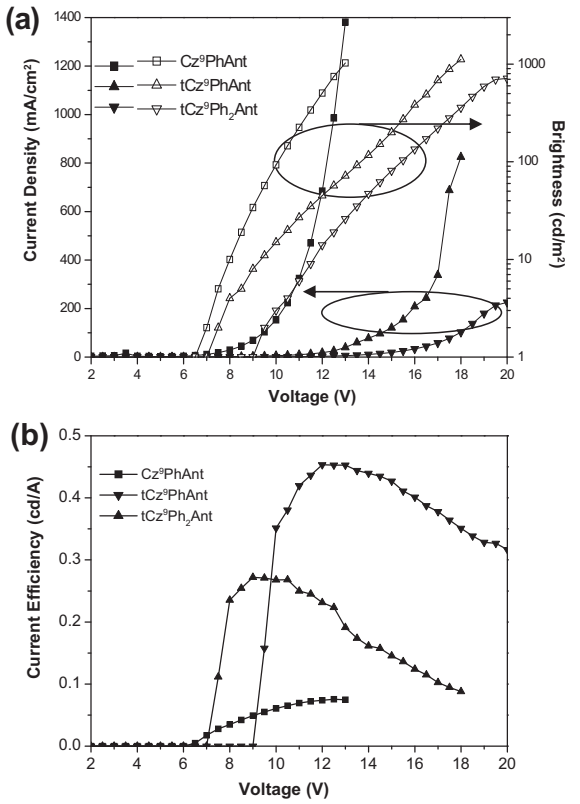

Fig. 5. EL performances of Cz^9PhAnt-, tCz^9PhAnt-, and tCz^9Ph_2Ant-based type-A devices.

Figs. 5 and 6 present the EL properties of the OLEDs based on the carbazole-substituted anthracene derivatives; Table 3 summarizes the key EL performance data of the non-doped devices. The EL performance of the triple-layer devices (type-B devices) was superior to that of the double-layer devices (type-A devices). The holes could be injected into the blue emitter layer more efficiently through the HTL (NPB layer) for the type-B devices. Nevertheless, the effect of the carbazole moieties on the EL performance of the type-A devices was the same as that for the type-B devices. For the type-B devices, the turn-on

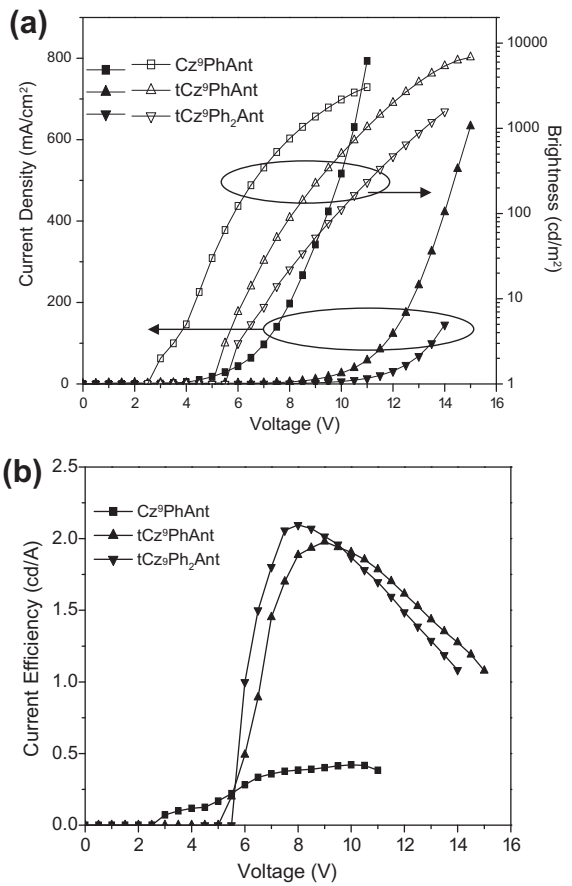

Fig. 6. EL performances of Cz^9PhAnt-, tCz^9PhAnt-, and tCz^9Ph_2Ant-based type-B devices.

voltages of the Cz^9PhAnt-, tCz^9PhAnt-, and tCz^9Ph_2Ant-based devices were 2.0, 5.0, and 5.5 eV, respectively. The tCz^9Ph_2Ant-based device (Device B-III) exhibited a maximum current efficiency of 2.10 cd/A and a maximum brightness of 1576 cd/m^2; for the tCz^9PhAnt-based device (Device B-II), these values were 1.98 cd/A and 6821 cd/m^2, respectively; for the Cz^9PhAnt-based device (Device B-I), they were 0.42 cd/A and 3042 cd/m^2, respectively. The Cz^9PhAnt-based device exhibited the lowest turn-on voltage among the three type-B devices. The presence of the *tert*-butyl groups reduced the charge transporting capacities of tCz^9PhAnt and tCz^9Ph_2Ant and resulted in higher turn-on voltages for their devices [23]. Moreover, the high value of Φ_{fl} and high coplanarity of Cz^9PhAnt led to the high current density and high brightness of the Cz^9PhAnt-based device. Nevertheless, the high coplanarity of Cz^9PhAnt in thin film state resulted in EL quenching in the device. As a result, the lowest current efficiency was that of the Cz^9PhAnt-based OLED. In addition, the tCz^9PhAnt-based devices exhibited higher brightnesses and larger current efficiencies relative to those of the Cz^9PhAnt-based device. The presence of *tert*-butyl groups on the carbazole moiety inhibited the aggregation and π–π^* stacking of the anthracene derivatives, thereby improving the EL performance of the OLEDs. As a result,

Table 3
EL properties of OLEDs incorporating the anthracene derivatives.

Compound	Device type	λ_{max}^{EL} (nm)	FWHM of EL at 10 V (nm)	V_{on} (V)[a]	Max. luminance (cd/m^2)	Max. efficiency (cd/A)	CIE (x, y)[b]
Cz^{9}PhAnt	Device A-I[c]	440	61	6.0	1030	0.08	(0.18, 0.15)
Cz^{9}PhAnt	Device B-I[d]	446	58	2.5	3042	0.42	(0.16, 0.11)
*t*Cz^{9}PhAnt	Device A-II	440	56	6.5	1120	0.27	(0.19, 0.14)
*t*Cz^{9}PhAnt	Device B-II	446	58	5.0	6821	1.98	(0.16, 0.12)
*t*Cz^{9}Ph$_2$Ant	Device A-III	446	52	9.0	714	0.45	(0.20, 0.17)
*t*Cz^{9}Ph$_2$Ant	Device B-III	452	62	5.5	1576	2.10	(0.17, 0.16)

[a] Turn-on voltage at 1 cd/m^2.
[b] Commission Internationale de L'Eclairage coordinates; under an applied voltage of 10 V.
[c] Device A: ITO/EML (70 nm)/TPBI (30 nm)/LiF/Al.
[d] Device B: ITO/NPB (40 nm)/EML (30 nm)/TPBI (30 nm)/LiF/Al.

the current efficiency of the *t*Cz^{9}PhAnt-based device was much higher than that of the Cz^{9}PhAnt-based device. On the other hand, the maximum current efficiency of the *t*Cz^{9}Ph$_2$Ant-based device was greater than that of the *t*Cz^{9}PhAnt device, while the current density and brightness followed the opposite trend. We attribute the higher current efficiency of the *t*Cz^{9}Ph$_2$Ant-based device to the greater conjugation of the biphenyl group linking the carbazole moiety to the anthracene derivative. The EL performances were, however, not only affected by the degree of conjugation of the molecule but also by the conformation and packing density of the emitter molecules in thin film state [23,25]. The lower current density and lower brightness of the *t*Cz^{9}Ph$_2$Ant-based device might have been due to poorer packing of these molecules. In addition, the presence of bipolar structure would bring about better charge balance of electron and hole, and further resulted in the higher EL performances for these carbazole-attached anthracene derivatives based devices [55,56].

Fig. 7 presents the EL spectra of the type-A (Devices A-I, A-II, and A-III) and type-B (Devices B-I, B-II, and B-III) devices. Table 3 summarizes the maximum emission wavelength of the EL (λ_{max}^{EL}), the FWHM of the EL signal, and the CIE coordinates of the devices based on these carbazole-substituted anthracene derivatives. We observed blue light with a value of λ_{max}^{EL} near 440–446 nm for the type-A devices. The values of FWHM for our three type-A devices ranged from 52 to 61 nm. These EL spectra are quite similar to the PL spectra of the carbazole-substituted anthracene derivatives in thin film state, apart from the FWHMs of device A-III. For compound *t*Cz^{9}Ph$_2$Ant, the FWHM (63 nm) of PL emission band was larger than that (52 nm) of EL emission band. The deviation of EL from its PL might be attributed to the electric-field or micro-cavity effects on the EL emission of *t*Cz^{9}Ph$_2$Ant-based device (Device A-III) [12,57]. Thus, the EL emissions arose predominantly from the carbazole-substituted anthracene derivatives. Notably, the values of λ_{max}^{EL} of the type-B devices were blue-shifted by 6 nm relative to those of the type-A devices. The influence of the chemical structure on the values of λ_{max}^{EL} of the type-B devices was consistent with the variations in the values of λ_{max}^{PL} of the anthracene derivatives. The FWHMs of the type-B devices differed slightly from those of the type-A devices. In this case, the effect of the chemical structure on the FWHM of the EL peaks was not consistent with the variation of the FWHMs

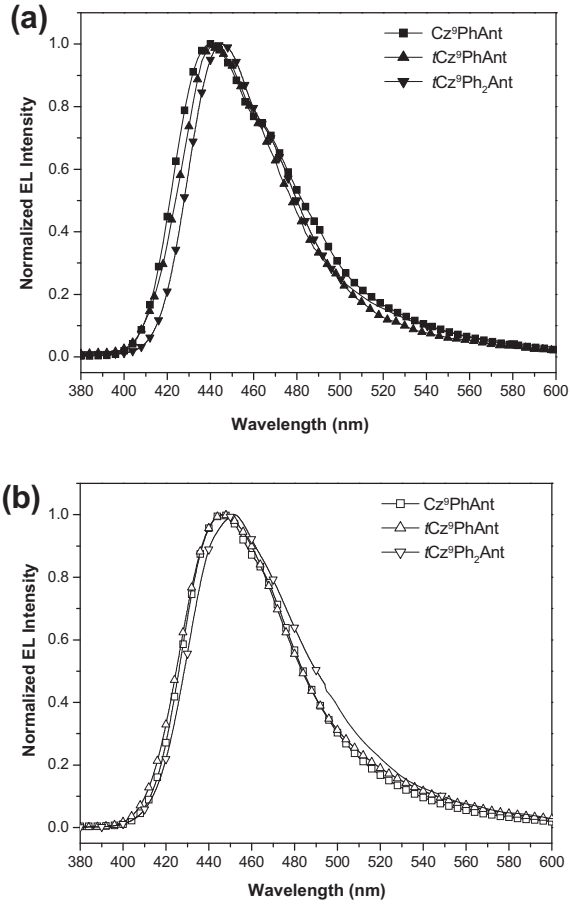

Fig. 7. EL spectra of Cz^{9}PhAnt-, *t*Cz^{9}PhAnt-, and *t*Cz^{9}Ph$_2$Ant-based devices under an applied voltage of 10 V (a) type-A devices; (b) type-B devices.

of the PL peaks of the anthracene derivatives, suggesting that the EL spectra of the OLEDs were affected by not only the chemical structure of blue emitter but also the thickness of the light emitting layer and the nature of the HTL and ETL materials [12]. For the type-A devices, the CIE color coordinates of Cz^{9}PhAnt-, *t*Cz^{9}PhAnt-, and *t*Cz^{9}Ph$_2$Ant-based devices were (0.18, 0.15), (0.19, 0.14), and (0.20, 0.17), respectively. The CIE color coordinates of the Cz^{9}PhAnt-, *t*Cz^{9}PhAnt-, and *t*Cz^{9}Ph$_2$Ant-based type-B

devices were (0.16, 0.11), (0.16, 0.12), and (0.17, 0.16), respectively – quite close to those of the standard blue emission (0.15, 0.15). Thus, the color purities of the type-B devices were higher than those of the type-A devices.

4. Conclusion

We have synthesized and characterized three blue-emitting anthracene derivatives – Cz^9PhAnt, tCz^9PhAnt, and tCz^9Ph_2Ant – featuring carbazole-substituted side-groups. The presence of 3,6-di-*tert*-butyl-9*H*-carbazole moieties prevented molecular aggregation of the anthracene derivatives, resulting in amorphous solid state structures. These anthracene derivatives exhibit high T_gs and, therefore, good thermal stability. Moreover, Cz^9PhAnt, tCz^9PhAnt, and tCz^9Ph_2Ant exhibit strong blue emissions in the form of thin films. From OLEDs fabricated using the carbazole-substituted anthracene derivatives as blue emitting layers, the brightnesses and current efficiencies for the tCz^9PhAnt- and tCz^9Ph_2Ant-based devices were greater than those of the Cz^9PhAnt-based device. The presence of *tert*-butyl groups on the carbazole moieties minimized the aggregation and π–π^* stacking of the anthracene derivatives, thereby improving the EL performances of the OLEDs. In addition, the Cz^9PhAnt-, tCz^9PhAnt-, and tCz^9Ph_2Ant-based OLEDs displayed high color purity. The EL performances of the devices based on these anthracene derivatives were strongly dependent on the chemical structure of the carbazole-based side-groups. We conclude that anthracene derivatives bearing carbazole moieties are useful emitting materials or hole-transporting/emitting materials in OLED architectures.

Acknowledgments

We thank the National Science Council (NSC) and the Ministry of Education, Taiwan, for financial support under the ATU plan.

References

[1] C.W. Tang, S.A. Vanslyke, Appl. Phys. Lett. 51 (1987) 913.
[2] J.H. Burroughes, D.D.C. Bradley, A.R. Brown, R.N. Marks, K. Mackay, R.H. Friend, P.L. Burns, A.B. Holms, Nature 347 (1990) 539.
[3] C.W. Tang, S.A. VanSlyke, C.H. Chen, J. Appl. Phys. 65 (1989) 3610.
[4] M.A. Baldo, M.E. Thompson, S.R. Forrest, Nature 403 (2000) 750.
[5] L.S. Hung, C.H. Chen, Mater. Sci. Eng. R 39 (2002) 143.
[6] T. Fuhrmann, J. Salbeck, MRS Bull. 28 (2003) 354.
[7] Y. Kijima, N. Asai, S. Tamura, Jpn. J. Appl. Phys. 38 (1999) 5274.
[8] A. Saitoh, N. Yamada, M. Yashima, K. Okinaka, A. Senoo, K. Ueno, D. Tanaka, R. Yashiro, SID 2004 Technical Digest 35 (2004) 150.
[9] M.T. Lee, C.H. Liao, C.H. Tsai, C.H. Chen, Adv. Mater. 17 (2005) 2493.
[10] T. Noda, H. Ogawa, Y. Shirota, Adv. Mater. 11 (1999) 283.
[11] Y. Shirota, M. Kinoshita, T. Noda, K. Okumoto, T. Ohara, J. Am. Chem. Soc. 122 (2000) 1102.
[12] L.H. Chan, R.H. Lee, C.F. Hsieh, H.C. Yeh, C.T. Chen, J. Am. Chem. Soc. 124 (2002) 6469.
[13] C.C. Wu, Y.T. Lin, K.T. Wong, R.T. Chen, Y.Y. Chien, Adv. Mater. 16 (2004) 61.
[14] S.W. Wen, M.T. Lee, C.H. Chen, J. Display Technol. 1 (2005) 90.
[15] C. Hosokawa, H. Higashi, H. Nakamura, T. Kusumoto, Appl. Phys. Lett. 67 (1995) 3853.
[16] S.J. Wang, W.J. Oldham, R.A. Hudack, G.C. Bazan, J. Am. Chem. Soc. 122 (2000) 5695.
[17] S.L. Lin, L.H. Chan, R.H. Lee, M.Y. Yen, W.J. Kuo, C.T. Chen, R.J. Jeng, Adv. Mater. 20 (2008) 3947.
[18] S.L. Tao, Z.K. Peng, X.H. Zhang, P.F. Wang, C.S. Lee, S.T. Lee, Adv. Funct. Mater. 15 (2005) 1716.
[19] S. Tao, Z. Hong, Z. Peng, W. Ju, X. Zhang, P. Wang, S. Wu, S. Lee, Chem. Phys. Lett. 397 (2004) 1.
[20] K. Danel, T.H. Huang, J.T. Lin, Y.T. Tao, C.H. Chuen, Chem. Mater. 14 (2002) 3860.
[21] P.I. Shih, C.Y. Chuang, C.H. Chien, E.W.G. Diau, C.F. Shu, Adv. Funct. Mater. 17 (2007) 3141.
[22] Y.Y. Lyu, J. Kwak, O. Kwon, S.H. Lee, D. Kim, C. Lee, K. Char, Adv. Mater. 20 (2008) 2720.
[23] S.K. Kim, Y.I. Park, I.N. Kang, J.W. Park, J. Mater. Chem. 17 (2007) 4670.
[24] J. Shi, C.W. Tang, Appl. Phys. Lett. 80 (2002) 3201.
[25] Y.H. Kim, H.C. Jeong, S.H. Kim, K. Yang, S.K. Kwon, Adv. Funct. Mater. 15 (2005) 1799.
[26] I.B. Berlan, Handbook of Fluorescence Spectra of Aromatic Molecules, second ed., Academic, New York, 1971.
[27] M.A. Reddy, A. Thomas, K. Srinivas, V.J. Rao, K. Bhanuprakash, B. Sridhar, A. Kumar, M.N. Kamalasanan, R. Srivastava, J. Mater. Chem. 19 (2009) 6172.
[28] S.L. Tao, Y.C. Zhou, C.S. Lee, S.T. Lee, D. Huang, X.H. Zhang, J. Phys. Chem. C 112 (2008) 14603.
[29] S.K. Kim, B. Yang, Y. Ma, J.H. Lee, J.W. Park, J. Mater. Chem. 18 (2008) 3376.
[30] J.Y. Park, S.Y. Jung, J.Y. Lee, Y.G. Baek, Thin Solid Films 516 (2008) 2917.
[31] Y.J. Pu, A. Kamiya, K.I. Nakayama, J. Kido, Org. Electron. 11 (2010) 479.
[32] W.J. Jo, K.H. Kim, H.C. No, D.Y. Shin, S.J. Oh, J.H. Son, Y.H. Kim, Y.K. Cho, Q.H. Zhao, K.H. Lee, H.Y. Oh, S.K. Kwon, Synth. Met. 159 (2009) 1359.
[33] S.K. Kim, B. Yang, Y.I. Park, Y. Ma, J.Y. Lee, H.J. Kim, J. Park, Org. Electron. 10 (2009) 822.
[34] C.H. Chien, C.K. Chen, F.M. Hsu, C.F. Shu, P.T. Chou, C.H. Lai, Adv. Funct. Mater. 19 (2009) 560.
[35] J.K. Park, K.H. Lee, S. Kang, J.Y. Lee, J.S. Park, J.H. Seo, Y.K. Kim, S.S. Yoon, Org. Electron. 11 (2010) 905.
[36] C.J. Zheng, W.M. Zhao, Z.Q. Wang, D. Huang, J. Ye, X.M. Ou, X.H. Zhang, C.S. Lee, S.T. Lee, J. Mater. Chem. 20 (2010) 1560.
[37] C.H. Wu, C.H. Chien, F.M. Hsu, P.I. Shih, C.F. Shu, J. Mater. Chem. 19 (2009) 1464.
[38] W.J. Kuo, S.L. Lin, S.D. Chen, C.P. Chang, R.H. Lee, R.J. Jeng, Thin Solid Films 516 (2008) 4145.
[39] J.A. Joule, Adv. Heterocycl. Chem. 35 (1984) 83.
[40] B.E. Koene, D.E. Loy, M.E. Thompson, Chem. Mater. 10 (1998) 2235.
[41] D.F. O'Brien, P.E. Burrows, S.R. Forrest, B.E. Koene, D.E. Loy, M.E. Thompson, Adv. Mater. 10 (1998) 1108.
[42] Y. Shirota, J. Mater. Chem. 10 (2000) 1.
[43] P. Kundu, K.R.J. Thomas, J.T. Lin, Y.T. Tao, C.H. Chien, Adv. Funct. Mater. 13 (2003) 445.
[44] K.R.J. Thomas, J.T. Lin, Y.T. Tao, C.W. Ko, J. Am. Chem. Soc. 123 (2001) 9404.
[45] Y. Liu, M. Nishiura, Y. Wang, Z.M. Hou, J. Am. Chem. Soc. 128 (2006) 5592.
[46] R.M. Adhikari, B.K. Shah, D.C. Neckers, J. Org. Chem. 74 (2009) 3341.
[47] F.A. Neugebauer, H. Fisher, S. Bamberger, H.O. Smith, Chem. Ber. 105 (1972) 2686.
[48] N.P.H. Nam, S.W. Cha, B.S. Kim, S.H. Choi, D.S. Choi, J.I. Jin, Synth. Met. 130 (2002) 271.
[49] L.L. Miller, G.D. Nordblom, E.A. Mayeda, J. Org. Chem. 37 (1972) 916.
[50] C.J. Yang, S.A. Jenekhe, Macromolecules 28 (1995) 1180.
[51] M.S. Workentin, L.J. Johnston, D.D.M. Wayner, V.D. Parker, J. Am. Chem. Soc. 116 (1994) 8279.
[52] H. Zhang, S. Wang, Y. Li, B. Zhang, C. Du, X. Wan, Y. Chen, Tetrahedron 65 (2009) 4455.
[53] S.Y. Ku, L.C. Chi, W.Y. Hung, S.W. Yang, T.C. Tsai, K.T. Wong, Y.H. Chen, C.I. Wu, J. Mater. Chem. 19 (2009) 773.
[54] C.C. Wu, Y.T. Lin, H.H. Chiang, T.Y. Cho, C.W. Chen, K.T. Wong, Y.L. Liao, G.H. Lee, S.M. Peng, Appl. Phys. Lett. 81 (2002) 577.
[55] C. Adachi, T. Tsutsui, S. Saito, Appl. Phys. Lett. 56 (1990) 799.
[56] X.Y. Jiang, Z.L. Zhang, X.Y. Zheng, Y.Z. Wu, S.H. Xu, Thin Solid Films 401 (2001) 251.
[57] Y. Fukuda, T. Watanabe, T. Wakimoto, S. Miyaguchi, M. Tsuchida, Synth. Met. 111–112 (2000) 1.